Acta Technica *62* No. 4B/2017, 1–8 © 2017 Institute of Thermomechanics CAS, v.v.i.

Design and fabrication of field effect transistor based on graphene as an explosive detector

Saeid Masoumi[1,5], Hassan Hajghassem[2], Alireza Erfanian[3], Ahmad Molaei Rad[4]

Abstract. We fabricated a bipolar field-effect transistors based on graphene and analyzed their performance. A field effect transistor includes a P-type semiconductor substrate as a back gate, graphene sheet is used as the channel material in device with transferring graphene sheet from Cu substrates to target substrates, source and drain electrodes formed at a distance 6 µm, and junctions between the source and drain electrodes and the semiconductor region are formed as an insulated area including a Schottky barrier. When the device was tested at room temperature, it exhibited V-shaped ambipolar transport properties with the minimum conductivity at around VGS∼1 V, charge neutrality point (CNP) where the electrons and holes are equal in density, from p-type region to n-type region. We have used biological receptor with a field effect transistor based on graphene to fabricate sensor for achieving high sensitivity and selectivity that can detect explosive substances such as TNT. The transport property changed compared to that of the FET made by intrinsic graphene, that is, the Dirac point position moved from positive Vg to negative Vg, indicating the transition of graphene from p-type to n-type after annealing in TNT, and our results show the bipolar property change of GFET with the TNT concentration and the possibility to develop a robust, easy-to-use, and low-cost TNT detection method for performing a sensitive, reliable, and semi-quantitative detection in a wide detection range. The results suggest that our method is fast, facile, and substrate independent.

Key words. Field effect transistor, electrode, graphene, bipolar.

1. Introduction

Selective and sensitive detection of explosives is very important in countering terrorist threats. Detecting trace explosives has become a very complex and expensive

[1]Department of Electronic Engineering, Tasouj Branch, Islamic Azad University, Tasouj, Iran
[2]Department of Faculty of New Sciences & Technologies, Tehran University, Iran
[3]Department of Electronic Engineering, Malek Ashtar University of Technology, Iran
[4]Department of Bioscience and Biotechnology, Malek Ashtar University of Technology, Iran
[5]Corresponding author; e-mail: S.masoumi.ee@gmail.com

endeavor because of a number of factors, such as the wide variety of materials that can be used as explosives, the lack of easily detectable signatures, the vast number of avenues by which these weapons can be deployed, and the lack of inexpensive sensors with high sensitivity and selectivity. High sensitivity and selectivity, combined with the ability to lower the deployment cost of sensors using mass production, is essential in winning the war on explosives-based terrorism. Many approaches have been explored for TNT detections. Current sensing methods of nitro-based explosives are gas and liquid chromatography [1], mass spectrometry [2], ion-mobility spectroscopy [3], enzymatic assays [4], and electrochemical detection [5]. Nanosensors have the potential to satisfy all the requirements for an effective platform for the trace detection of explosives. In 2000, Kong et al. first demonstrated a nanomaterial-based gas sensor [6]. During the past decades, nanomaterial-based FET biosensors, such as one-dimensional (1D) Si Nano-wire (SiNW), carbon nanotube (CNT) and graphene devices have attracted significant attention for label-free detection of chemical and biological species. Carbon has various crystalline allotropes such as diamond, graphite, graphene and nanotubes. The carbon atoms in diamond are sp3 hybridized and sp2 hybridized in the rest of them. Graphene is a two-dimensional network of carbon atoms arranged on a honeycomb lattice. A stack of graphene sheets bound by weak van der Waals forces is graphite. A graphene sheet rolled into a tube is a carbon nanotube (CNT). A graphene sheet with at least 12 pentagonal defects results in fullerene. Graphene was not known to exist in isolated form until 2004 when it was first isolated by Novoselov's group in Manchester [7].

2. Methodology

2.1. Graphene transfer process

The first step necessary in fabricating devices GFET is to transfer the graphene from the metal Cu substrate onto a device-compatible substrate. Monolayer Graphene on Cu (10 mm×10 mm) with thickness (theoretical) 0.345 nm is purchased from Graphenea of Spain. It is crucial to device performance, yield, and uniformity that the quality of the graphene is not degraded during this transfer process. Thus, in an ideal transfer process, the graphene film should remain clean, with no contamination and continuous without folds, cracks, or holes. After coating PMMA, the Cu is etched away by iron nitrate; the transparent PMMA/graphene stack usually floats on the solution surface as shown in Fig. 1.

After etching of the copper foil, graphene/PMMA was put into distilled water for 10 minutes and rinsed. Then ionic and heavy metal atomic contaminants were removed by using a solution of 25:1:1 $H_2O/H_2O_2/HCl$ and cleaning the residual metal particles remaining on the PMMA/graphene stack. The PMMA/graphene stack was rinsed by DI water. The next stage was intended for the removal of insoluble organic contaminants with a 25:1:1 $H_2O/H_2O_2/NH_4OH$ solution. To avoid damaging the graphene/PMMA stack in the bubbles created by the H_2O_2, the process of washing was done at room temperature. After each etching step, the PMMA/graphene stack was rinsed by DI water. To transfer the graphene/PMMA stack, the substrate with

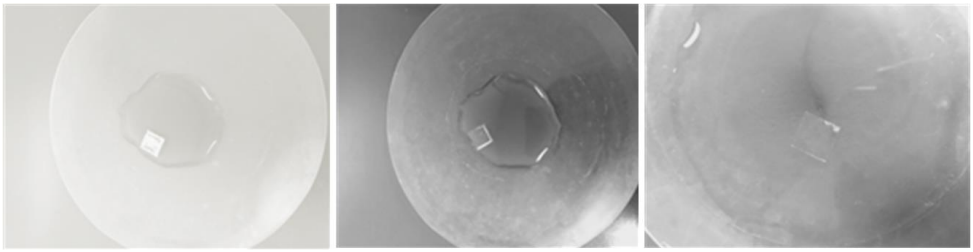

Fig. 1. Etching of copper foil, PMMA/graphene stack floats on the solution surface

piranha solution was activated. Piranha solution (750 micro liters of H_2O_2 with 250 micro liters of sulfuric acid) increases its hydrophilicity due to an increase in the density of the OH groups on the $Si/SiO_2/Cr$ surface and improves the smoothness of the graphene/PMMA. The increase in the hydrophilicity significantly reduces the formation of large folds and wrinkles, and the PMMA/graphene stack can be transferred without large fold formation onto the target substrate. After the transfer of the graphene/PMMA stack to the substrate, the residual water was dried thoroughly, the sample was baked at 150 °C for 15 min to evaporate it and improve the contact between the stack and the substrate as shown in Figure 2. PMMA is then removed by solvent rinsing (such as acetone or n-methylpyrrolidinone, (NMP)). Typically after PMMA removal, the sample is put to the Si/SiO_2/graphene in vacuum sputtering with argon gas at a temperature of 300 °C for 20 minutes to be used to further improve the graphene/substrate contact and remove residual particles of PMMA. In the end of the step of transfer, the sample was cleaned with acetone, IPA, DI water, and then dried using low pressure ultra high purity N_2.

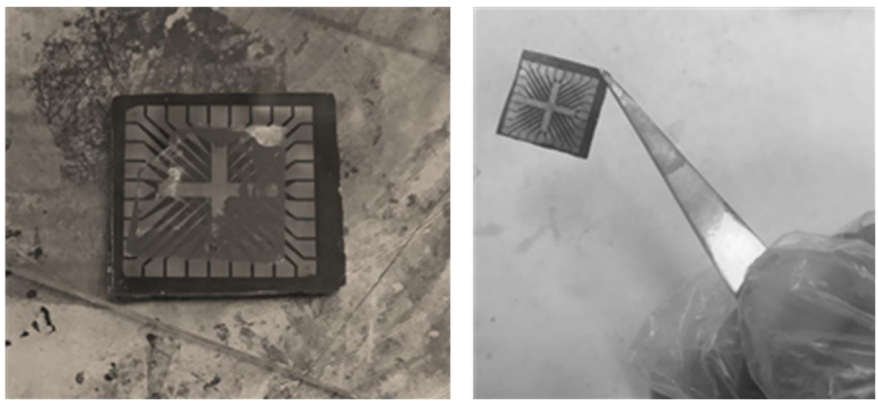

Fig. 2. Transfer of graphene/PMMA stack on $Si/SiO_2/Cr$ marker substrate with water bubbles. Baking of the $Si/SiO_2/Cr$ markers/graphene/PMMA for evaporating water bubbles and improving contact between the stack and the substrate

Following this process, a clean and almost crackless graphene film can be transferred to various target substrates.

2.2. Raman spectra

Raman spectroscopy is a powerful tool to characterize the structure and defects of carbon materials including carbon nanotubes and graphene. The Z scan is used to focus the laser on the sample surface. The peak position and height of the Raman spectra are known to depend on the number of layers in graphene. The Raman spectrum, optical image and SEM image of the graphene is shown in Fig. 4. The spectrum displays the D band and G band.

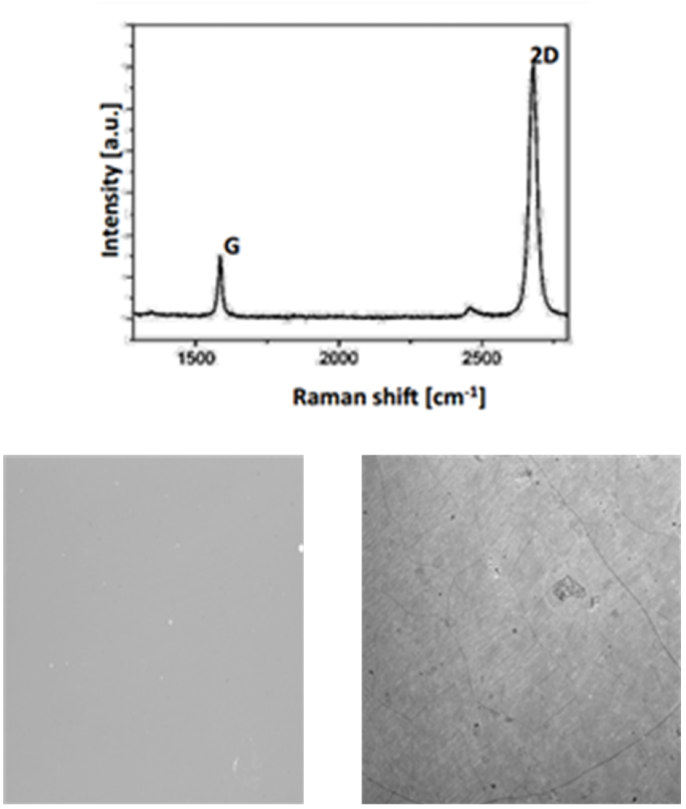

Fig. 3. Typical Raman spectra of graphene after Cu etching and transfer graphene sheet onto substrate (left), and optical microscopy image (middle) and SEM image (right) of the graphene

The transferred graphene film is very clean, with almost no residual particles seen under optical microscope.

2.3. Patterning of graphene sheet & Fabrication of the electrodes (S/D)

After the patterning of the graphene sheet with DIRE and O_2 plasma, the metal source/drain contacts were patterned to form FETs with a $60\times6\,\mu m^2$ and $30\times6\,\mu m^2$

channel area where the Si-substrate was used as a back gate. Graphene FETs were fabricated (drain-source electrodes 110 nm Au on 30 nm Cr) by standard photolithography processes based on a widely used photoresist, Shipley 1813. After metal deposition, lift-off was performed at 80 °C by soaking the sample in Remover 1165 (1-methyl-2-pyrrolidinone) and then thoroughly rinsed with isopropyl alcohol. An important feature of lift processes is that the side wall profile of the photoresist must be vertical or with an overhang. This causes a break in the deposited metal film and ensures easy lift-off. After normal lithography the side walls are sloped, and in order to get an overhang profile, the lithographic process is altered slightly. A toluene (formerly chlorobenzene) soak step is included after the UV exposure but before development. The toluene hardens the top layers of the photo resist making them harder to develop away. In general, the exposure time and the development time need to be changed from the optimal conditions to account for the alteration of the resist properties due to the toluene soak. After the expose sample to UV light, immerse the sample in a beaker containing toluene for 1 minute and do not rinse the sample in DI H_2O after the toluene soak. Then now develop the photoresist and the other standard lithography process can be continued. The result of placing the sample in toluene is shown in Fig. 4. The mask and optical microscopy images of the source and drain electrodes with SEM images of the GFETs are illustrated in Fig. 5.

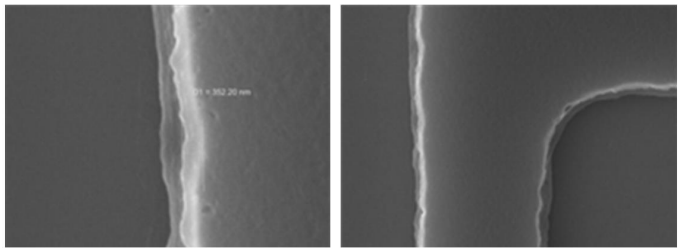

Fig. 4. Sample in toluene solution for 2 (left) and 1 (right) minutes

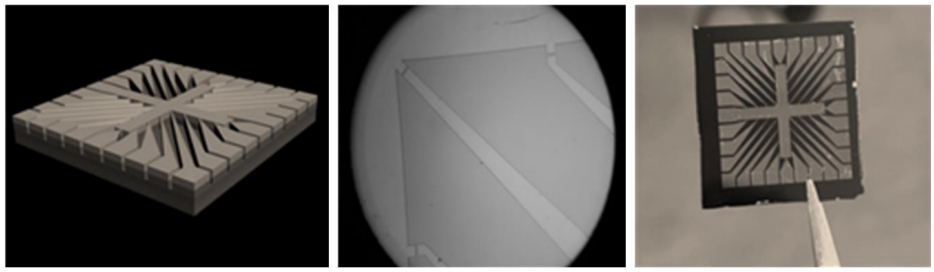

Fig. 5. Left–the mask of the source and drain electrodes ($Si/SiO_2/Cr/Au$, graphene as a channel, 31 transistor samples with different dimensions), middle–the SEM and optical microscopy images of the source/drain electrodes, right–the sample made of GFETs

3. Results

Finally, the target TNT is applied onto the device and then a silver wire is used as the gate to realize a gated GFET for electrical measurements. The source-drain current and back-gate voltage ($I_{\mathrm{ds}} - V_{\mathrm{g}}$) curves of the pristine graphene FET measured in air are depicted in Fig. 6 and show bipolar transistor effect, and the minimal conduction corresponds to the Dirac point (V_{dirac}).

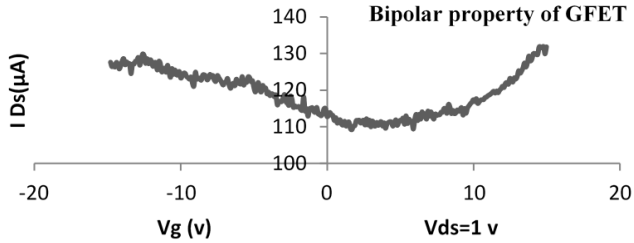

Fig. 6. $I_{\mathrm{ds}} - V_{\mathrm{g}}$ curve of the pristine graphene FET

When $V_{\mathrm{g}} < V_{\mathrm{dirac}}$, it operates as a p-channel FET, and for $V_{\mathrm{g}} > V_{\mathrm{dirac}}$, the device operate as an n-channel FET. In our transport measurement, the graphene annealed in TNT after irradiation shows distinguishing transport features in air (Fig. 7) compared with the pristine graphene FET and FET. Figure 7 shows, when the GFET sensor is coated with PDA without receptor, the electrical current of the sensor exhibits almost no changes to various concentrations of TNT molecules. In principle, the $\pi - \pi$ interactions of the (Trp-His-Trp) & TNT causes n-doping of the devices due to graphene. We could see that the biploar property of the GFETs shifts toward the left with increased concentration of the TNT, and this result is in good agreement with that described by other reports [6].

4. Conclusion

In summary, we have studied clean methods for transferring graphene from Cu substrates to target substrates and fabricated the GFET based on graphene. The graphene/wafer-substrate interface resulting from this clean transfer process is greatly improved. Laboratory results shows that the number of cracks in transferred graphene films can be reduced by controlling the hydrophilicity of the target substrate and baking. Graphene as the conducting material shows the obvious ambipolar characteristics at a small range of gate voltage on the back-gated FET devices under ambient conditions, and the devices are highly responsive to the low gate voltage. In order to functionalize the manufactured GFETs as a sensor with ability of recognizing the explosive TNT, the biological receptors were designed and synthesized. We have developed a rapid and selective TNT sensor based on FET with nanomaterials with good sensitivity and selectivity through the combination of GFETs and PDA-based lipid membranes coupled with biologically inspired TNT peptide receptors to significantly improve selectivity in a Nano electronic device sen-

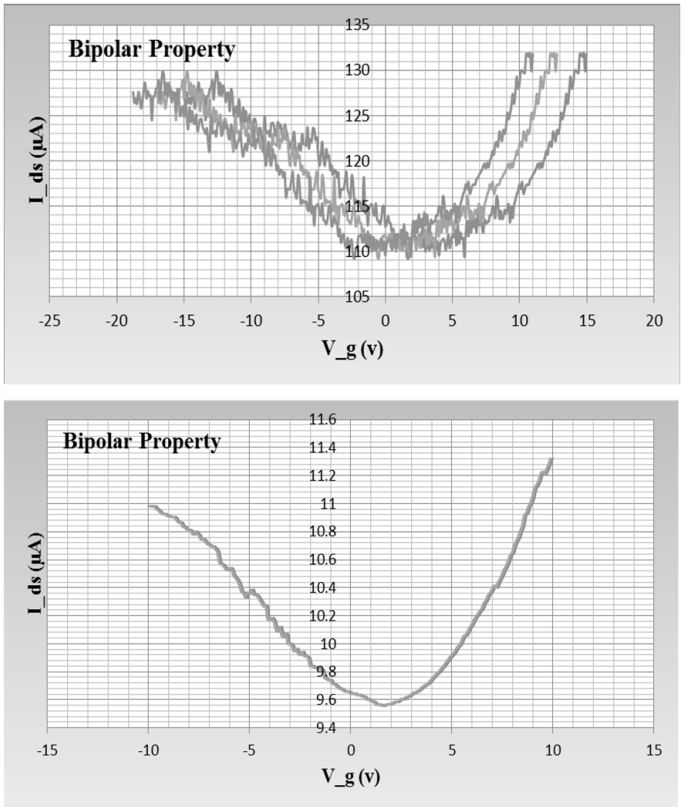

Fig. 7. $I_{\mathrm{ds}} - V_{\mathrm{g}}$ curves of graphene annealed in TNT after irradiation in GFETs: top–curves are measured at $V_{\mathrm{sd}} = 1\,\mathrm{V}$, bottom– GFET sensor coated with PDA without receptor and no changes in bipolar property curve

sor. Apply various types of explosives to the sensor, does not show that any response to non-target molecules and only in the presence target molecules of TNT reacts. Sensor recognition accuracy is at an acceptable level. Design and manufacturing of explosives detector sensors based on GFETs that is capable of responding to several different types of explosives in real time is the next thing the research group will publish in this journal.

References

[1] M. J. Davies, A. C. Thomas: *Plaque fissuring–the cause of acute myocardial infarction, sudden ischaemic death, and crescendo angina.* BMJ, Heart Journals *53* (1985), No. 4, 363–373.

[2] D. Liepsch: *An introduction to biofluid mechanics–basic models and applications.* Journal of Biomechanics *35* (2002), No. 4, 415–435.

[3] C. Tu, M. Deville: *Pulsatile flow of non-Newtonian fluids through arterial stenoses.* Journal of Biomechanics *29* (1996), No. 7, 899–908.

[4] S. Chien: *Hemorheology in clinical medicine.* Recent Advances in Cardiovascular Diseases (1981), Suppl. 2, 21–26.

[5] J. C. Misra, M. K. Patra, C. S. Misra: *A non-newtonian fluid model for blood flow through arteries under stenotic conditions.* Journal of Biomechanics *26* (1993), No. 9, 1129–1141.

[6] S. Chakravarty, P. K. Mandal: *Two-dimensional blood flow through tapered arteries under stenotic conditions.* International Journal of Non-Linear Mechanics *35* (2000), No. 5, 779–793.

[7] P. K. Mandal: *An unsteady analysis of non-Newtonian blood flow through tapered arteries with a stenosis.* International Journal of Non-Linear Mechanics *40* (2005), No. 1, 151–164.

[8] Sarifuddin, S. Chakravarty, P. K. Mandal: *Numerical simulation of Casson fluid flow through differently shaped arterial stenoses.* Zeitschrift für angewandte Mathematik und Physik *65* (2014), No. 4, 767–782.

[9] K. L. Moore: *Clinically oriented anatomy.* Williams and Wilkins, Baltimore, MD (1990).

[10] R. L. Whitemore: *Rheology of Circulation.* Pergamon Press, Oxford, UK (1968).

[11] G. Porenta, G. F. Young, T. R. Rogge: *A finite-element model of blood flow in arteries including taper, branches and obstructions.* ASME Journal of Biomechanical Engineering *108* (1986), No. 2, 161–167.

[12] J. Malek, K. R. Rajagopal, M. Ruzicka: *Existence and regularity of solutions and stability of the rest state of fluids with shear dependent viscosity.* Mathematical Models and Methods in Applied Sciences *5*(1995), No. 6, 789–812.

[13] J. L. Bansal: *Viscous fluid dynamics.* Oxford & IBH Publishing Company (1992), 74–76.

[14] R. Mittal, S. P. Simmons, H. S. Udaykumar: *Application of large-eddy simulation to the study of pulsatile flow in a modeled arterial stenosis.* ASME Journal of Biomechanical Engineering *123* (2003), No. 4, 325–332.

[15] D. Tang, C. Yang, S. Kobayashi, D. N. Ku: *Generalized finite difference method for 3-D viscous flow in stenotic tubes with large wall deformation and collapse.* Applied Numerical Mathematics *38* (2001), Nos. 1–2, 49–68.

Received May 7, 2017